Geophysical Research Letters

RESEARCH LETTER
10.1029/2019GL085280

A See-Saw in Pacific Subantarctic Mode Water Formation Driven by Atmospheric Modes

A. J. S. Meijers[1], I. Cerovečki[2], B. A. King[3], and V. Tamsitt[4,5]

[1]British Antarctic Survey, Cambridge, UK, [2]Scripps Institution of Oceanography, La Jolla, CA, USA, [3]National Oceanography Centre, Southampton, UK, [4]University of New South Wales, Sydney, New South Wales, Australia, [5]Centre for Southern Hemisphere Oceans Research, CSIRO Oceans and Atmosphere, Hobart, Tasmania, Australia

Key Points:
- South Pacific Subantarctic Mode Water (SAMW) layers display large (±150 m) changes in thickness from year to year
- Two distinct pools of South Pacific SAMW exist and their thicknesses see-saw out of phase with one another
- The phase and magnitude of variability are set by changes in wind stress and heat flux driven by the main atmospheric modes of variability

Supporting Information:
- Supporting Information S1

Correspondence to:
A. J. S. Meijers,
andmei@bas.ac.uk

Citation:
Meijers, A. J. S., Cerovečki, I., King, B. A., & Tamsitt, V. (2019). A see-saw in Pacific Subantarctic Mode Water formation driven by atmospheric modes. *Geophysical Research Letters*, *46*, 13,152–13,160. https://doi.org/10.1029/2019GL085280

Received 4 SEP 2019
Accepted 21 OCT 2019
Accepted article online 11 NOV 2019
Published online 16 NOV 2019

Abstract Subantarctic Mode Water (SAMW) in the Pacific forms in two distinct pools in the south central and southeast Pacific, which subduct into the ocean interior and impact global storage of heat and carbon. Wintertime thickness of the central and eastern SAMW pools vary predominantly out of phase with each other, by up to ±150 m between years, resulting in an interannual thickness see-saw. The thickness in the eastern (central) pool is found to be strongly positively (negatively) correlated with both the Southern Annular Mode (SAM) and El Niño–Southern Oscillation (ENSO). The relative phases of the SAM and ENSO set the SAMW thickness, with in phase reinforcing modes in 2005–2008 and 2012–2017 driving strong differences between the pools. Between 2008 and 2012 out of phase atmospheric modes result in less coherent SAMW patterns. SAMW thickness is dominated by local formation driven by SAM and ENSO modulated wind stress and turbulent heat fluxes.

Plain Language Summary The Southern Ocean around Antarctica is a dominant pathway for moving heat and carbon from the atmosphere into the ocean interior, trapping it for hundreds of years. Most of this uptake is achieved through the formation of "mode waters", homogeneous layers of water several hundred meters thick, by sinking and overturning as surface waters cool in winter. We find that two distinct pools of mode water in the South Pacific vary dramatically in winter thickness and volume from year to year. They vary in opposition to one another; when one is thicker than normal the other is thinner, with the pattern reversing after a year or so. We show that this "see-saw" in thickness is strongest when the two main atmospheric patterns of climate variability over the Southern Ocean are reinforcing one another and weaken when they oppose one another. The combination of these patterns of atmospheric variability sets local mode water thickness via surface winds and ocean heat loss. The discovery of such strong dependence of mode water heat content on these atmospheric patterns is important for climate. Atmospheric variability is predicted to change into the future, potentially impacting heat uptake by mode waters and influencing global surface temperatures.

1. Introduction

SubAntarctic Mode Water (SAMW) formation is the key process in the Southern Ocean whereby surface waters are subducted into the thermocline, transporting heat, CO_2, and nutrients to intermediate ocean depths where they are subsequently exported northward (Marshall & Speer, 2012). SAMW forms on the equatorward side of the subantarctic front, primarily through intense winter surface heat loss and subsequent formation of deep mixed layers (Figure 1a). These deep mixed layers do not form uniformly around the Southern Ocean and instead appear in large "pools" primarily in the southern Indian Ocean, south of Australia, and in the central and eastern South Pacific (McCartney, 1982). The spatial structure of these pools leads to distinct regional subducted SAMW export pathways (Jones et al., 2016; Sallée et al., 2010), ventilating each basin's subtropical gyres with varying densities of mode water with distinct properties (Herraiz-Borreguero & Rintoul, 2011). Since Argo observations began, changes in SAMW formation rates and properties have driven the most significant anthropogenic heat uptake by the global ocean anywhere on the planet, accounting for 67–98% of the net global ocean heat uptake, which itself is the dominant component of the global climate system warming (Roemmich et al., 2015; Frölicher et al., 2015). This increase in heat uptake is driven largely by increased formation rates and increases in the volume of the SAMW layer, rather than significant changes in the temperature of the SAMW itself (Gao et al., 2018). Understanding the processes

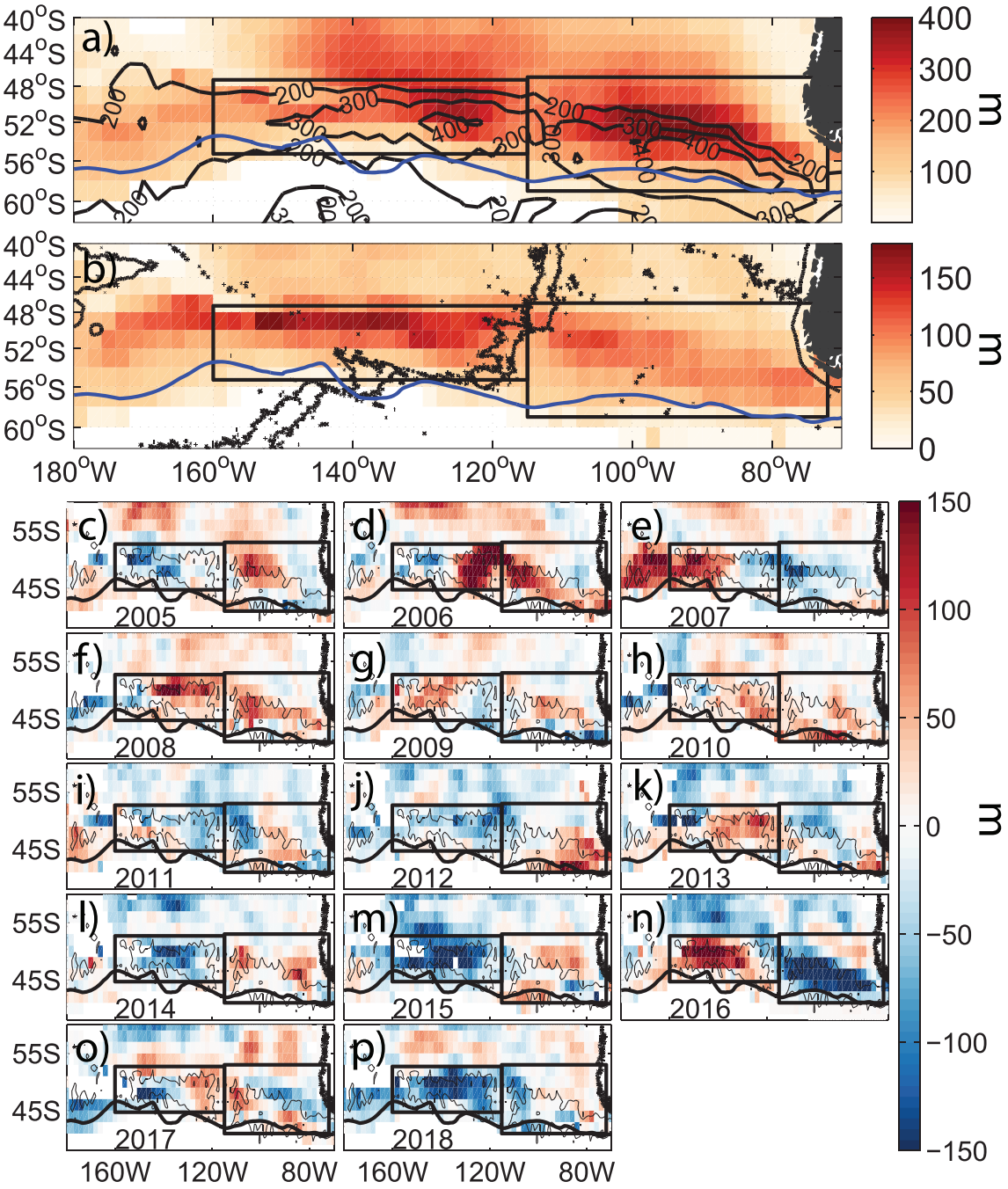

Figure 1. (a) SAMW winter (JAS) mean thickness (m) for 2005–2018 with mean mixed layer depth contoured. (b) As in (a) but for SAMW standard deviation (m) with 3,000 m isobaths contoured. (c–p) Gridded SAMW wintertime (JAS) thickness anomalies by year. Fine contour indicates the position of the 400 m maximum Mixed Layer Depth (MLD). In all panels bold boxes indicate the position of the eastern and central regions referred to through the manuscript. The bold climatological position of the subantarctic front (Kim & Orsi, 2014) marks the southern boundary of deep SAMW formation regions.

that set the thickness and formation rates of SAMW is therefore of great importance if we are to understand both how recent climate change has driven the observed ocean heat uptake, as well as predict how this may change in the future under various climate change scenarios.

Argo-based mapping of Southern Ocean properties onto a regular gridded climatology (Roemmich et al., 2009) revealed intense interannual variability in the properties of SAMW in the South Pacific in years 2005–2010 (Cerovečki et al., 2019). The variability is concentrated in the regions of deep winter mixed layers in the southeast and central Pacific, where SAMW is initially formed before being subducted into the interior

(Sallée et al., 2010). As newly formed SAMW is advected away from these formation zones it carries the signal of variability into the ocean interior. This region is of particular importance in setting ocean interior properties in both the Pacific (Jones et al., 2016) and the South Atlantic (Meredith et al., 2008; Naveira Garabato et al., 2009). It is located close to the atmospheric "pole of variability" where the maximum sea level pressure variability is noted (Connolley, 1997). Ocean surface properties, wintertime heat loss, and mixed layer depth in the region are strongly influenced by the resulting variable wind strength and direction (Ogle et al., 2018). Two primary modes dominate atmospheric variability in the South Pacific: the Southern Annular Mode (SAM) and El Niño–Southern Oscillation (ENSO) (Hall & Visbeck, 2002; Turner, 2004).

In this paper we use a new gridded time-evolving climatology of Argo hydrographic data to characterize the year-to-year spatial and temporal variably of SAMW in the South Pacific (section 3). In section 4 we link these changes to the primary modes of atmospheric variability in this region, the SAM and ENSO, and in section 5 we use ERA-Interim atmospheric reanalysis datasets to uncover the mechanisms by which the SAMW is modified. We discuss the findings and present conclusions in section 6.

2. Materials and Methods

2.1. Argo Data and Mapping

The mapped Argo data product was created by objective mapping of temperature and salinity anomalies relative to a World Ocean Atlas (WOA) climatology, following Desbruyères et al. (2014, 2017). Data were obtained from the Argo Global Data Assembly Center (GDAC) snapshot 8 January 2019: https://doi.org/10.17882/ (Argo, 2019). Anomalies from these raw Argo profiles collected over 2005–2018 were calculated relative to the monthly WOA 2013 climatology (Locarnini et al., 2013; Zweng et al., 2013) and mapped on a vertical pressure grid with 100 levels at 20-dbar spacing. Data-data and data-grid covariances used a 500 km length scale, equal in every direction. Mapped anomalies were then recombined with the climatology to produce the mapped fields. Data were mapped onto a 2° × 2° grid, with a 10 day time base from 2005 to 2018. To avoid biases common in conventional objective mapping (e.g., Bretherton et al., 1976), the weights were normalized so that at each grid point and time step, the weights to be applied to observation anomalies had a sum of unity, regardless of the number of observations and distance of the observations from the grid point. In the period and region of analysis the number of profiles available to map each grid point varied from 3 to 60 with a mean of 23, and 95% of grid points have 10 or more profiles available.

2.2. Other Data Sets

Also used are sea level pressure, wind stress, and heat flux fields from 2005 to 2018, from the ERA-Interim atmospheric reanalysis project developed by the European Centre for Medium-Range Weather Forecasts (https://doi.org/10.5065/D6CR5RD9). The SAM (https://legacy.bas.ac.uk/met/gjma/sam.html, Marshall, 2003) and ENSO Nino 3.4 (https://www.esrl.noaa.gov/psd/data/correlation/nina34.data) indexes are obtained for the same period.

2.3. Definition of SAMW Volume and Formation Regions

The SAMW was defined similarly to Cerovečki et al. (2019). SAMW was classified as any water with a potential density $26.85 < \sigma_\theta < 27.1$ kg m^{-3} and a potential vorticity $<30 \times 10^{-12}$ m^{-1} s^{-1}, although unlike Cerovečki et al. (2019) only a single SAMW density class is used over the whole South Pacific. The regions of SAMW formation, the central Pacific box (143–114°W, 47.3–55.3°S) and eastern Pacific box (114–72°W, 47–59°S), are the same as those in Cerovečki et al. (2019) and are chosen as they are regions of local maximum winter mixed layer depth and contain distinctly varying SAMW pools (Figures 1a and 1b), possibly due to the presence of the Pacific Antarctic Ridge at approximately 115°W.

3. Results

3.1. SAMW Volume Variability

Although SAMW is a climatologically persistent layer several hundred meters thick (Figure 1a), Argo observations reveal that the thickness of SAMW, defined as in section 2.3, varies significantly from one austral winter (July–September, JAS) to the next (Figure 1). The winter thickness anomaly varies by up to ±150 m each year, with the greatest magnitude and most coherent signals appearing in the deep winter mixed layer regions where SAMW forms: north of the subantarctic front and extending to around 47°S. Equatorward of this the

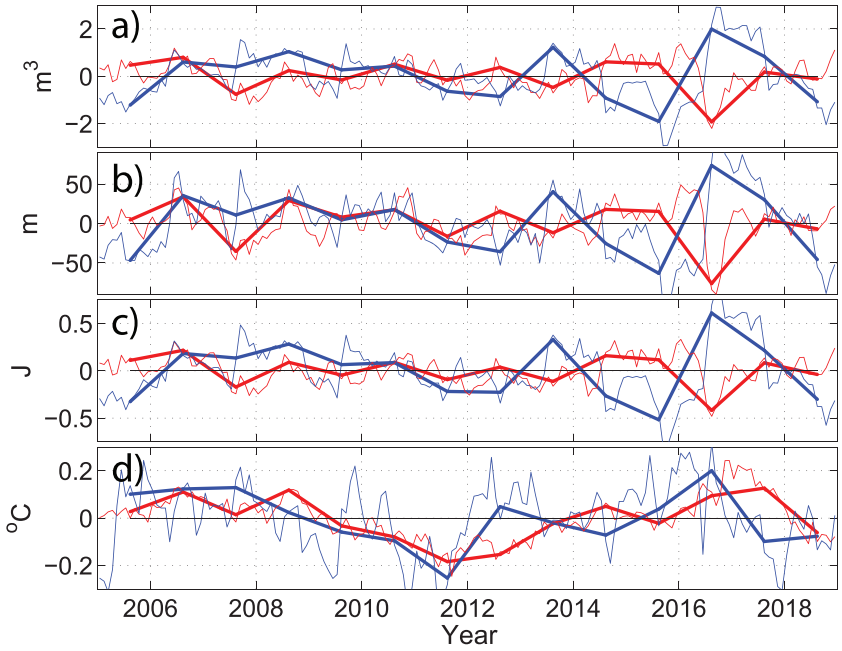

Figure 2. Detrended monthly mean anomaly of (a) volume ($\times 10^{14}$ m^3), (b) thickness (m), (c) net heat content ($\times 10^{22}$ J), and (d) volume weighted potential temperature (°C) of SAMW for east (red) and central (blue) regions. Bold lines link JAS mean values.

SAMW layer thickness is less variable from year to year (typically less than ±50 m, Figure 1b) and is not clearly correlated with the changes within the formation zones. From 2012 to 2018 there is a very distinct zonal separation between SAMW thickness anomalies at approximately 115°W, where the Pacific-Antarctic Ridge intersects the SAMW formation region (Figure 1b). At the longitudes above the ridge the maximum winter mixed layer depth is shallower than 300 m (Figure 1a). Between 2005 and 2008 strong anomalies are apparent as in post 2012, though they are not as clearly separated at 115°W, except in 2005. Between 2008 and 2012 there is still significant zonal variation in SAMW thickness anomalies, but it is noisier and of smaller magnitude without the clear split at 115°W.

To quantify the variability on the two sides of 115°W, we consider two SAMW formation regions as defined in Cerovečki et al. (2019) and referred to here as the "central" and "eastern" regions (see boxes in Figure 1) and calculate the detrended, volume-weighted, monthly mean SAMW properties within them. The interannual variability in SAMW thickness, rather than spatial extent, dominates the volume anomaly of SAMW in both regions and volume and thickness anomalies covary tightly in both the eastern and central region (Figures 2a and 2b). While there are significant month-to-month changes in SAMW properties, the winter mean (defined here over JAS) accurately captures the major peaks and troughs of the signal, reflecting the importance of this period for SAMW formation. Prior to 2008, the wintertime SAMW volume anomaly is mostly of opposite signs in the eastern and central Pacific. From 2008 to 2012 both regions exhibit remarkably similar net anomalies and their variability is correlated ($r^2 = 0.70$, p value $= 0.19$ for winter means, $r^2 = 0.26$, $p = 0.02$ for monthly means). In contrast, after 2012 the magnitude of mean thickness anomalies increases to greater than ±50 m in both regions and are clearly anticorrelated ($r^2 = -0.76$, $p = 0.05$), even on monthly timescales ($r^2 = -0.53$, $p < 0.001$). Additionally each region displays significant interannual changes, oscillating up to 100 m between years, with maximum anomalies in both eastern and central regions occurring in the austral winter of 2016. The variability in SAMW thickness calculated from the optimally interpolated product agrees with the same metric calculated using only raw Argo profiles (Figure S1 in the supporting information).

3.2. SAMW Property Variability

The change in SAMW thickness, rather than variability in temperature (Figure 2d), dominates net SAMW heat content anomalies (Figure 2c). This is consistent with recent trends in SAMW heat content found by

Gao et al., 2018. The very strong (>0.9) correlation between thickness and heat content implies that changes in the horizontal extent of SAMW in the central/eastern pools does not significantly impact volume. In contrast to heat content, SAMW potential temperature displays anomalies that persist for 2–3 years (Figure 2d). In addition to varying over longer periods, the wintertime mean temperature anomalies of SAMW differ from heat content in that the eastern and central regions exhibit a lagged positive correlation, rather than anticorrelation. The eastern pool lag of approximately one year behind the central pool are consistent with the findings of Cerovečki et al. (2019) who show that anomalies are advected along the ACC/subtropical gyre from the central to eastern Pacific over approximately 1 year. Meredith et al. (2008) observe a similar eastward progression of sea surface temperature anomalies via lagged correlations.

4. Relationship to Atmospheric Modes of Variability

The dominant modes of atmospheric variability in the South Pacific are the SAM and ENSO. These exert a strong influence on regional ocean properties (Naveira Garabato et al., 2009), circulation (Sallee et al., 2008), sea ice extent (Haumann et al., 2016), regional winds (Turner et al., 2017), and air-sea heat fluxes (Ogle et al., 2018). The map of regional regression of SAMW winter thickness onto the ENSO (Niño3.4) and SAM indexes is striking in its relationship to the central and eastern pools of variability (Figures 3a and 3b). Within the central and eastern boxes there are coherent and strong regions of statistically significant correlation ($r^2 > 0.6$, $p < 0.05$) for both SAM and ENSO. Each mode is positively correlated with SAMW thickness in the eastern region and negatively in the central Pacific. In both cases the region of correlation is strongest on the northern side of the deep mixed layer formation sites and extends equatorward of the boxes as far as 45°S. This pattern also matches the first EOF of SAMW winter thickness (capturing 49.6% of the variance) (Figure S2).

Each atmospheric mode has approximately equal impact on SAMW thickness, with changes of up to ±50 m for a single standard deviation in either index. In contrast to thickness the SAMW mean potential temperature has a weaker correlation with either atmospheric mode, although the qualitative split into eastern and central pools of opposite signs is similar (Figure S3).

Correlations of thickness with both SAM and ENSO peak at 0–2 months lag and decay over the following 6–12 months (Figure S4a). There are secondary, weaker, correlations of thickness for both SAM and ENSO between 12 and 24 months lag of the opposite sign to those at zero lag. ENSO (but not SAM) has strong statistically significant correlations with SAMW temperature anomalies. These peak at 3–5 months lag in the central Pacific, and then a year later at 15 months lag in the eastern Pacific (Figure S4b). These lags are consistent with those noted in Meredith et al. (2008) and Naveira Garabato et al. (2009), and with the hypothesis that SAMW mode water anomalies are advected from central to eastern Pacific over the course of approximately 1 year (see section 6 and Cerovečki et al., 2019).

Combined with these strong relationships, the time series of the SAM and ENSO indexes (Figure 3c) suggests that the interplay of the relative phase and strength of the two atmospheric indexes corresponds with the thickness and properties of South Pacific SAMW. Between 2005 and 2018 the two indexes move in and out of phase with one another. Based on the correlations in Figure 3, and if a causal (and linear) relationship exists, when the atmospheric modes are in phase they will reinforce and drive the central and eastern pools into opposite signed anomalies, and while out of phase their influence will cancel, driving weak net variability and little covariance.

From 2005 to late 2007 the two indexes are largely in phase. From 2008 to 2012 they are largely out of phase, with a particularly strong La Niña in 2010 coinciding with a strong positive SAM. After late 2012 the two indexes are again in phase, culminating in a strong El Niño event in early 2016 coincident with a strong positive SAM. Both indexes transition to strongly negative by austral winter 2016. This pattern of in-out-in phase corresponds well to the variability of SAMW thickness and volume over the whole time series (Figure 2). Composites of a subset of mean winter SAMW thicknesses according the phase and sign of SAM and ENSO produces strongly coherent patterns that agree with the Figure 3 regression relationship when in phase and noisy patterns when out of phase (Figure S5).

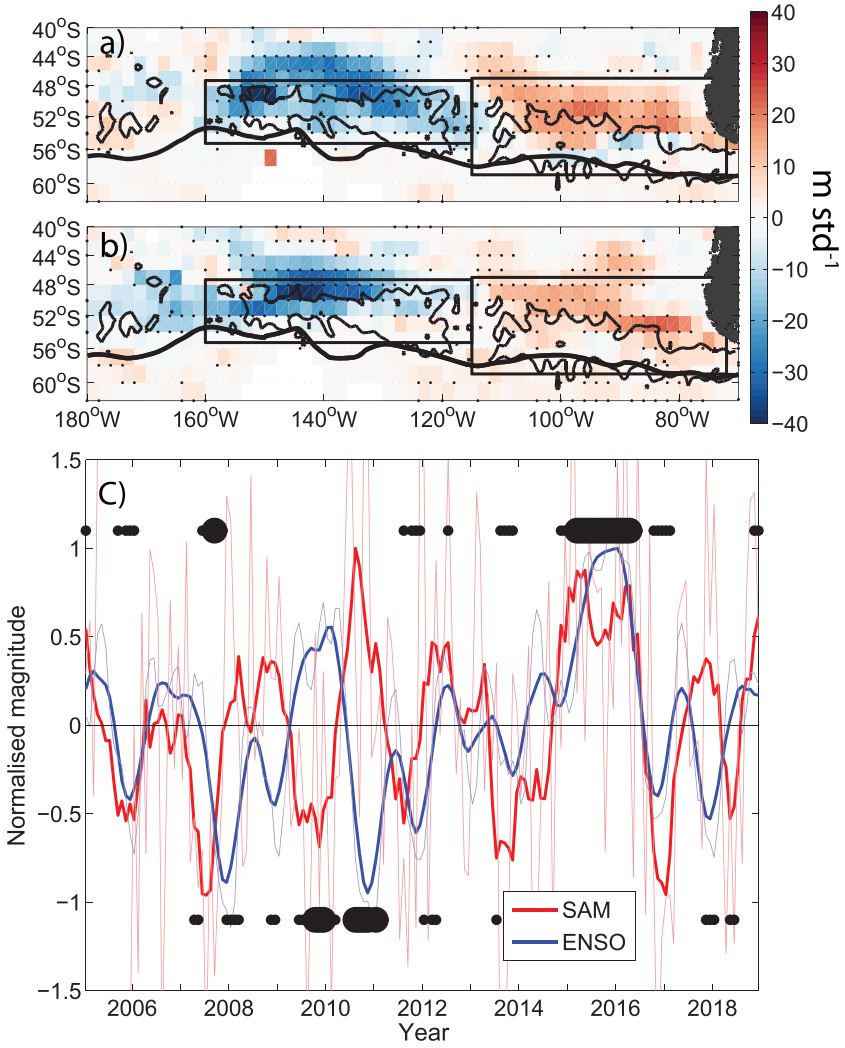

Figure 3. (a) ENSO and (b) SAM regression onto detrended SAMW thickness anomalies 2005–2018. Each index is normalized by one standard deviation to give indicative impact on thickness (i.e., meters per standard deviation of the index, m std^{-1}). Stippling indicates a statistically significant correlation at the 95% level. (c) Normalized monthly SAM (red) and ENSO3.4 (blue). Bold lines indicate three month running mean of index. Positive (negative) black dots indicate when SAM and ENSO are in (out of) phase and at least one exceeds one standard deviation in magnitude, and large black dots indicate when both exceed one standard deviation in magnitude.

5. Mechanisms Driving SAMW Property Change

The above results show that the relative strength and sign of the large scale SAM and ENSO atmospheric modes are strongly correlated with the variability in thickness and volume of the two SAMW pools in the South Pacific. To understand the actual physical mechanisms driving the variance, we examine the relationship of wind stress with SAMW thickness. The SAM has a distinct relationship to wind stress (Thompson & Solomon, 2002), driving a poleward shift and increase in strength of the westerly jet in its positive phase (Figure 4a). The ENSO influences high latitudes via several mechanisms, with a strong wave number one teleconnection with sea level pressure in the southeast Pacific (Turner et al., 2017) and the Amundsen Sea Low (Turner et al., 2013). Positive (negative) ENSO events result in southerly (northerly) wind anomalies confined to the eastern SAMW formation region (Figure 4d). Changes in wind stress may alter the mixed layer properties and depth through both changes in the lateral advection of water (Rintoul & England, 2002) vertical Ekman pumping and heave and changes in the wintertime turbulent heat loss via changes in the overlying air temperature and humidity (Ogle et al., 2018).

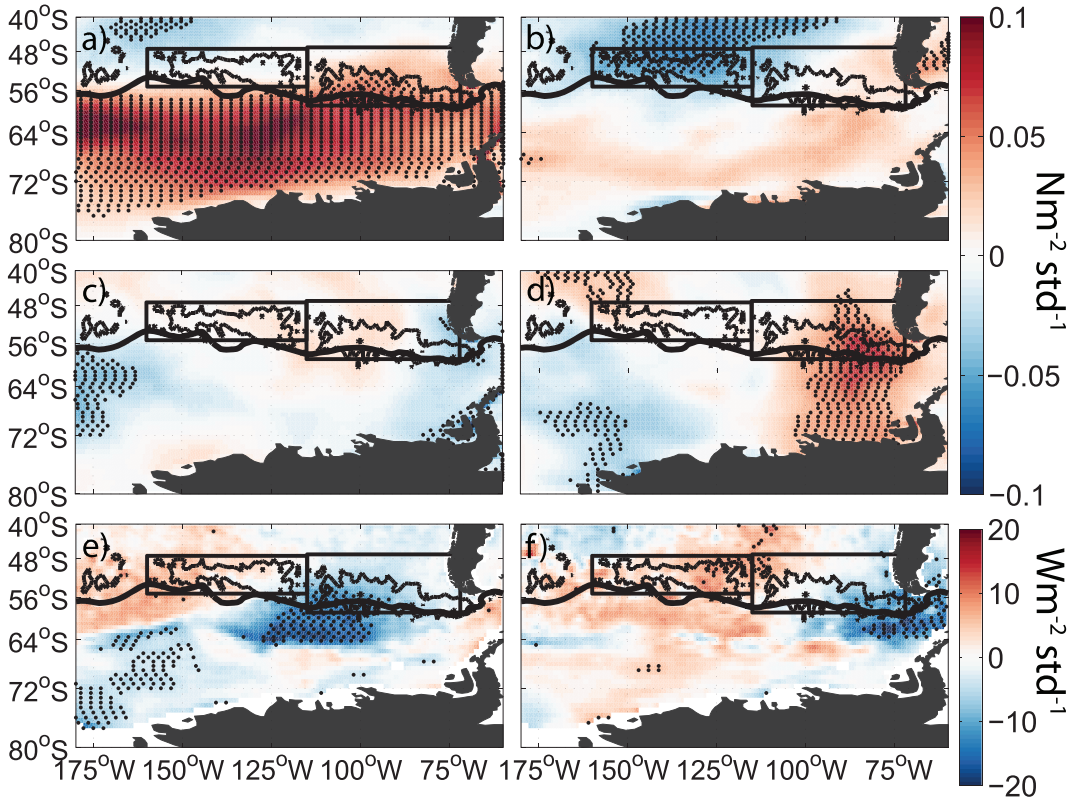

Figure 4. Regression of (a, c, and e) SAM and (b, d, and f) ENSO onto (a, b) zonal, (c, d) meridional wind stress, and (e, f) net heat fluxes for winters (JAS) 2005–2017. Each index is normalized by one standard deviation to give indicative impact on wind stress (N m^{-2} std^{-1}) and heat flux (W m^{-2} std^{-1}). Stippling indicates a correlation significant at the 95% level.

When the SAM is positive in austral winter the strongest correlation in the region is with zonal wind stress (Figure 4a). This is concentrated largely poleward of 55°S resulting in the more southerly eastern SAMW pool experiencing stronger zonal wind stress and potentially deeper mixed layers via enhanced mixing and Ekman advection. In contrast there is little statistically significant relationship between the SAM and zonal winds over the central pool or meridional winds anywhere in the region (Figures 4a and 4c). The ENSO in its positive (negative) phase drives more easterly (westerly) winds over the central pool and more southerly (northerly) winds over the eastern pool (Figures 4b and 4d). When the correlation is carried out over the full seasonal cycle these patterns remain consistent (Figure S6).

A similar pattern emerges when looking at the response of the net surface heat flux in the region to SAM and ENSO variability (Figures 4e and 4f). A positive SAM is associated with enhanced heat loss over the eastern box and consequent convection and a deeper mixed layer, while in the central box there is surface warming (Figure 4e). Similarly, under positive ENSO conditions there is anomalous ocean heat uptake and SAMW thinning in the central box, while heat loss is enhanced in the eastern box. These patterns align with the wind stress regression onto SAMW (Figures 4a–4d), although the spatial structure is not as clearly separated at 115°W in the heat flux case. Splitting the net heat loss into its component terms, we find that sensible and latent heat loss are the dominant drivers in this relationship (Figures S7 and S8). The similarity between wind and turbulent heat flux anomalies is not unexpected as latent/sensible heat fluxes are directly dependent on wind speed, and air temperature and humidity is affected by meridional wind direction. While freshwater fluxes are known to also be important in SAMW formation, the net ERA-Interim winter buoyancy flux anomaly is dominated by the heat flux component over both the central and eastern boxes (Figure S9). This agrees with Cerovečki et al. (2013) who find that in the southeast Pacific SAMW formation is dominated by cooling rather than freshening.

6. Discussion and Conclusion

This analysis demonstrates the clear dominance of the relative phase of the SAM and ENSO atmospheric modes in driving both the spatial and the temporal variability of SAMW volume and heat content in the South Pacific. The new pressure mapping of Argo data demonstrates a dramatic see-saw in SAMW thickness between the central and eastern Pacific SAMW pools, varying out of phase with one another by up to ±150 m on yearly timescales. When both SAM and ENSO are in phase and positive (negative), the enhanced (reduced) westerly wind component of SAM drives a deepening (shoaling) of the eastern SAMW pool, reinforced by enhanced southerly (northerly) winds driven by ENSO. At the same time the easterly (westerly) anomaly in zonal winds driven by ENSO will shoal (deepen) the central SAMW pool, resulting in the eastern and central pools experiencing distinct thickness anomalies of opposite signs. When SAM and ENSO are out of phase, the resulting wind anomalies will oppose one another, resulting in much less coherent spatial signals. This strongly suggests that it is the spatial and temporal variance of wind stress that controls the observed changes in SAMW properties and thickness on annual timescales, as well as on previously identified decadal scales (Gao et al., 2018). The change in atmospheric temperature, humidity, and air-sea heat fluxes associated with the spatial structure of the wind stress anomalies reinforces the SAMW variability. This is particularly strong in the case of ENSO where it is associated with the strengthening or weakening of the wave one pattern in atmospheric pressure centered around 120°W, 65° S (Turner et al., 2017) (Figure S10b). A positive ENSO raises sea level pressure at this location and drives enhanced southerly winds over the eastern box. This brings cool air over the eastern SAMW formation zones, enhancing heat loss and subsequent deepening of the mixed layers. In contrast the central box receives enhanced warmer northerly winds off the subtropics, shoaling the mixed layers. These findings are backed up by the dominance of the turbulent heat flux terms in setting wintertime ocean heat loss and agree with the analysis of Ogle et al. (2018) based on in situ air-sea flux mooring data. This pattern of wind stress driving a dipole over the eastern and central SAMW pools dominates both meridional wind stress and net heat flux variability, and their first EOF mode captures over 55% and 61% of their variance, respectively (Figure S2). It is worth noting that other atmospheric modes do influence the region, notably zonal wave number 3 (ZW3). However, other studies note that ZW3 is strongly correlated with SAM (Turner et al., 2017) and we therefore focus our analysis on the dominant modes.

The impact of the strong spatial structure of atmospheric forcing on the temperature of SAMW in the region is less clear. The primary timescale of SAMW temperature variability is 2–5 years, with a ~1 year lag between the upstream central Pacific and downstream east Pacific, suggesting a dominant role for advection in setting regional properties with weaker responses to local atmospheric forcing superimposed. This aligns with other studies that have noted the importance of the background eastward flow in advecting anomalies generated by atmospheric and Ekman forcing (Verdy et al., 2006) and the approximate rate of advection between central and eastern Pacific (Meredith et al., 2008; Naveira Garabato et al., 2009). Cerovečki et al. (2019) similarly show that advection of freshwater on multiyear timescales from sea ice melt can be an important factor influencing SAMW properties in this region.

This lagged advective relationship between the central and downstream eastern Pacific also exists for SAMW thickness (Figure S4a), but it does not appear to dominate over the influence of local instantaneous austral winter air-sea fluxes and nor is there a coherent multiannual variability in thickness of the sort seen in the SAMW temperature. This result indicates that it is regional changes in primarily winter time air-sea heat flux and wind stress that set MLDs and SAMW thickness, though the role of advection in preconditioning water masses prior to winter convection merits further examination. It is important to note that while SAMW thickness and temperature variances respond on different spatial and temporal scales, it is the thickness of these water masses that dictates the net heat uptake (Figure 2). This is in accordance with Gao et al. (2018) who show the trend in heat uptake of SAMW is dominated by volume change rather than water mass warming.

The finding that SAMW heat uptake is intensely regional, strongly variable across the South Pacific, and highly dependent on the relative phase of the primary atmospheric modes has implications for future heat and carbon uptake. Changes in the location or relative magnitudes of these primary atmospheric modes, such as the projected increase of the SAM under climate forcing scenarios, may therefore have significant impact on regional water mass structure, as well as the magnitude and pathways of heat, carbon, and

nutrient uptake. Further work on both the processes controlling SAMW formation and its overall role in ocean heat and carbon uptake are required to understand how such changes may impact global climate.

Acknowledgments
A. M. and B. K. were supported by Natural Environment Research Council (NERC) grants NE/N018095/1 (Ocean Regulation of Climate by Heat and Carbon Sequestration and Transports; ORCHESTRA). I. C. was supported by the National Science Foundation (NSF) Ocean Sciences grant NSF OCE-1658001 to Scripps Institution of Oceanography. V.T. acknowledges support from CHSOR; CSHOR is a joint research center for Southern Hemisphere Ocean Research between QNLM and CSIRO. Data used in this work may be freely obtained from the websites listed in the Data and Methods section. Argo data were collected and made freely available by the International Argo Program and the national programs that contribute to it. (http://www.argo.ucsd.edu, http://argo.jcommops.org). The Argo Program is part of the Global Ocean Observing System. The Argo gridded product described in section is available for download at ftp://ftp.bas.ac.uk/pub/andmei/Argo_mappings/S_pac.

References

Argo (2019). Argo float data and metadata from Global Data Assembly Centre (Argo GDAC). https://doi.org/10.17882/42182

Bretherton, F. P., Davis, R. E., & Fandry, C. B. (1976). A technique for objective analysis and design of oceanographic experiments applied to MODE-73. *Deep Sea Research and Oceanographic Abstracts*, *23*, 559–582.

Cerovečki, I., Meijers, A. J., Mazloff, M. R., Gille, S. T., Tamsitt, V. M., & Holland, P. R. (2019). The effects of enhanced sea ice export from the Ross Sea on recent cooling and freshening of the Southeast Pacific. *Journal of Climate*, *32*, 2013–2035.

Cerovečki, I., Talley, L. D., Mazloff, M. R., & Maze, G. (2013). Subantarctic Mode Water formation, destruction, and export in the eddy-permitting Southern Ocean State Estimate. *Journal of Physical Oceanography*, *43*, 1485–1511. https://doi.org/10.1175/JPO-D-12-0121.1

Connolley, W. M. (1997). Variability in annual mean circulation in southern high latitudes. *Climate Dynamics*, *13*, 745–756.

Desbruyères, D., McDonagh, E. L., King, B. A., & Thierry, V. (2017). Global and full-depth ocean temperature trends during the early twenty-first century from argo and repeat hydrography. *Journal of Climate*, *30*(6), 1985–1997. https://doi.org/10.1175/jcli-d-16-0396.1

Desbruyères, D. G., McDonagh, E. L., King, B. A., Garry, F. K., Blaker, A. T., Moat, B. I., & Mercier, H. (2014). Full-depth temperature trends in the northeastern Atlantic through the early 21st century. *Geophysical Research Letters*, *41*, 7971–7979. https://doi.org/10.1002/2014gl061844

Frölicher, T. L., Sarmiento, J. L., Paynter, D. J., Dunne, J. P., Krasting, J. P., & Winton, M. (2015). Dominance of the Southern Ocean in anthropogenic carbon and heat uptake in CMIP5 models. *Journal of Climate*, *28*, 862–886. https://doi.org/10.1175/JCLI-D-14-00117.1

Gao, L., Rintoul, S. R., & Yu, W. (2018). Recent wind-driven change in Subantarctic Mode Water and its impact on ocean heat storage. *Nature Climate Change*, *8*, 58.

Hall, A., & Visbeck, M. (2002). Synchronous variability in the southern hemisphere atmosphere, sea ice, and ocean resulting from the annular mode. *Journal of Climate*, *15*, 3043–3057.

Haumann, F. A., Gruber, N., Münnich, M., Frenger, I., & Kern, S. (2016). Sea-ice transport driving Southern Ocean salinity and its recent trends. *Nature*, *537*, 89.

Herraiz-Borreguero, L., & Rintoul, S. R. (2011). Subantarctic mode water: Distribution and circulation. *Ocean Dynamics*, *61*, 103–126.

Jones, D. C., Meijers, A. J., Shuckburgh, E., Sallée, J.-B., Haynes, P., McAufield, E. K., & Mazloff, M. R. (2016). How does Subantarctic Mode Water ventilate the Southern Hemisphere subtropics? *Journal of Geophysical Research: Oceans*, *121*, 6558–6582. https://doi.org/10.1002/2016JC011680

Kim, Y. S., & Orsi, A. H. (2014). On the variability of Antarctic Circumpolar Current fronts inferred from 1992–2011 altimetry. *Journal of Physical Oceanography*, *44*, 3054–3071. https://doi.org/10.1175/JPO-D-13-0217.1

Locarnini, R. A., Mishonov, A. V., Antonov, J. I., Boyer, T. P., Garcia, H. E., Baranova, O. K., et al. (2013). In S. Levitus & A. Mishonov (Eds.), *World Ocean Atlas 2013, Volume 1: Temperature*, NOAA Atlas NESDIS (Vol. *73*, p. 40).

Marshall, G. J. (2003). Trends in the Southern Annular Mode from observations and reanalyses. *Journal of Climate*, *16*, 4134–4143. https://doi.org/10.1175/1520-0442(2003)016<4134:TITSAM>2.0.CO;2

Marshall, J., & Speer, K. (2012). Closure of the meridional overturning circulation through Southern Ocean upwelling. *Nature Geoscience*, *5*, 171–180.

McCartney, M. S. (1982). The subtropical recirculation of mode waters. *Journal of Marine Research*, *40*, 64.

Meredith, M. P., Garabato, A. C. N., Gordon, A. L., & Johnson, G. C. (2008). Evolution of the deep and bottom waters of the Scotia Sea, Southern Ocean, during 1995-2005. *Journal of Climate*, *21*, 3327–3343.

Naveira Garabato, A. C., Jullion, L., Stevens, D. P., Heywood, K. J., & King, B. A. (2009). Variability of Subantarctic Mode Water and Antarctic Intermediate Water in the Drake Passage during the late-twentieth and early-twenty-first centuries. *Journal of Climate*, *22*, 3661–3688.

Ogle, S. E., Tamsitt, V., Josey, S. A., Gille, S. T., Cerovečki, I., Talley, L. D., & Weller, R. A. (2018). Episodic Southern Ocean heat loss and its mixed layer impacts revealed by the farthest south multiyear surface flux mooring. *Geophysical Research Letters*, *45*, 5002–5010. https://doi.org/10.1029/2017GL076909

Rintoul, S. R., & England, M. H. (2002). Ekman transport dominates local air-sea fluxes in driving variability of Subantarctic mode water. *Journal of Physical Oceanography*, *32*, 1308–1321.

Roemmich, D., Church, J., Gilson, J., Monselesan, D., Sutton, P., & Wijffels, S. (2015). Unabated planetary warming and its ocean structure since 2006. *Nature Climate Change*, *5*(3), 240–245. https://doi.org/10.1038/nclimate2513

Roemmich, D., Johnson, G., Riser, S., Davis, R., Gilson, J., Owens, W. B., et al. (2009). The Argo Program: Observing the global ocean with profiling floats. *Oceanography*, *22*(2), 34–43. https://doi.org/10.5670/oceanog.2009.36

Sallee, J.-B., Speer, K., & Morrow, R. (2008). Response of the Antarctic Circumpolar Current to atmospheric variability. *Journal of Climate*, *21*, 3020–3039.

Sallée, J. B., Speer, K., Rintoul, S. R., & Wijffels, S. (2010). Southern Ocean thermocline ventilation. *Journal of Physical Oceanography*, *40*, 509–529.

Thompson, D. W. J., & Solomon, S. (2002). Interpretation of recent southern hemisphere climate change. *Science*, *296*(5569), 895–899. https://doi.org/10.1126/science.1069270

Turner, J. (2004). The El Niño–Southern Oscillation and Antarctica. *International Journal of Climatology*, *24*, 1–31.

Turner, J., Orr, A., Gudmundsson, G. H., Jenkins, A., Bingham, R. G., Hillenbrand, C.-D., & Bracegirdle, T. J. (2017). Atmosphere-ocean-ice interactions in the Amundsen Sea Embayment, West Antarctica. *Reviews of Geophysics*, *55*, 235–276. https://doi.org/10.1002/2016RG000532

Turner, J., Phillips, T., Hosking, J. S., Marshall, G. J., & Orr, A. (2013). The Amundsen Sea low. *International Journal of Climatology*, *33*, 1818–1829.

Verdy, A., Marshall, J., & Czaja, A. (2006). Sea surface temperature variability along the path of the Antarctic Circumpolar Current. *Journal of Physical Oceanography*, *36*, 1317–1331.

Zweng, M. M., Reagan, J. R., Antonov, J. I., Locarnini, R. A., Mishonov, A. V., Boyer, T. P., et al. (2013). In S. Levitus & A. Mishonov (Eds.), *World Ocean Atlas 2013, Volume 2: Salinity*, NOAA Atlas NESDIS (Vol. 74, p. 39).